Hindawi Publishing Corporation
International Journal of Photoenergy
Volume 2014, Article ID 425836, 8 pages
http://dx.doi.org/10.1155/2014/425836

Research Article

Enhanced Transformation of Atrazine by High Efficient Visible Light-Driven N, S-Codoped TiO_2 Nanowires Photocatalysts

Yanlin Zhang,[1,2,3] Honghai Wu,[1,2] and Peihong Liu[1]

[1] *School of Chemistry and Environment, South China Normal University, Guangzhou 510006, China*
[2] *Key Laboratory of Theoretical Chemistry of Environment Ministry of Education, South China Normal University, Guangzhou 510006, China*
[3] *Guangdong Technology Research Center for Ecological Management and Remediation of Urban Water System, School of Chemistry & Environment, South China Normal University, Guangzhou 510006, China*

Correspondence should be addressed to Yanlin Zhang; zhangyl@scnu.edu.cn

Received 15 July 2014; Accepted 17 September 2014; Published 19 October 2014

Academic Editor: Hongtao Yu

Advanced oxidation process using titanium dioxide as a photocatalyst under solar irradiation is one of the most attractive technologies to eliminate atrazine, an endocrine disrupting and carcinogen contaminant. The N, S-codoped TiO_2 nanowires at the calcination of 600°C obtained by a facile hydrothermal method revealed the best photocatalytic performance for the degradation of atrazine under visible light irradiation compared to N, S-codoped TiO_2 nanoparticles and S-doped TiO_2 nanowires. TOC removal experiment also exhibited the similar result and achieved 63% of atrazine mineralization within 6 h. The degradation of atrazine was driven mainly by $^{\bullet}OH$ and holes during the photocatalytic process. Reactive species quantities such $^{\bullet}OH$ and $O_2^{\bullet-}$ generated by N, S-codoped TiO_2 nanowires under visible light irradiation were much more than those of S-doped TiO_2 nanowires and N, S-codoped TiO_2 nanoparticles. These results were mainly attributed to the synergistic effect of N and S doping in narrowing the band gap, remarkable increase in electron-hole separation, extending the anatase-to-rutile transformation temperature above 600°C, and preferentially exposing high reactive {001} crystal facets of anatase.

1. Introduction

Atrazine is a kind of triazine herbicides widely used for crops and weed control and is classified as a possible human carcinogen by the USEPA [1]. The features of atrazine such as slow hydrolysis, low vapor pressure, moderate aqueous solubility, and atrazine resistance to microbial degradation enhance its potential of leaching into groundwater and soil [2]. The release of atrazine into natural ecosystem has caused endocrine disrupting and carcinogen concerns for human. The persistence of atrazine is due to the stability of the s-triazine ring; thus cyanuric acid, ammelide, and ammeline were generally recognized as the end products [3–5]. Therefore, effective treatment processes to enhance the degradation of atrazine or complete mineralization are urgently needed.

Various studies were developed to enhance the degradation efficiency of atrazine by using advanced oxidation processes (AOPs), which include photolysis of hydrogen peroxide [6], Fenton process [7], UV/Fenton [8], electrochemical-Fenton [9], and catalytic ozonation [10].

Solar irradiation using TiO_2 has also been applied in photocatalytic processes for water and wastewater treatment [11]. It is well known that TiO_2 is one of the most attractive photocatalysts owing to its superior redox ability, long-term stability against chemical and photochemical corrosion, and low toxicity. But its wide band gap of 3.2 eV for anatase and 3.0 eV for rutile restricts its application as a photocatalyst under visible light. The development of new advanced photocatalysts that exhibits high reactivity under visible light is a great challenge.

Doping has been considered as an effective method by modifying the electronic structure of TiO_2 to extend the spectral response of TiO_2 to the visible region [12–17] and anionic doping was confirmed to be more effective to suppress localization of the d states of titanium deep in the band gap of

TiO_2 than cationic doping. Doping TiO_2 with an appropriate combination of nonmetals would result in more visible light sensitive photocatalysts for a desired application because of the synergistic effect tuning the electronic structure [18, 19].

Among nanoscale materials, one-dimensional (1D) structure of such material is greatly desired as it has higher charge carrier mobility and lower carrier recombination rate. The speed of electron diffusion across nanoparticle junctions is several orders of magnitude smaller than that of 1D crystalline material due to frequent electron trapping at the junctions of nanoparticles [20]. In this case, separated charges are easily recombined before they reach the surface of nanoparticles.

In this paper, the as-prepared N, S-codoped TiO_2 nanowires (NS-TiO_2 NWs) by hydrothermal method were used to enhance the degradation of atrazine. We found that NS-TiO_2 NWs have better photocatalytic properties for TOC removal than S-doped TiO_2 NWs (S-TiO_2 NWs) or N, S-codoped TiO_2 nanoparticles (NS-TiO_2 NPs) irritated by visible light for degradation of atrazine. We further researched the degradation kinetics, reactive species and discussed the reasons of photocatalytic activity enhancement by NS-TiO_2 NWs.

2. Experimental

2.1. Materials. Atrazine (>98.9%) was purchased from Chem Service Inc. All the other solvents and chemicals were of analytical grade. Titanium sulfate, thiourea, tert-butyl alcohol (TBA), ethylenediaminetetraacetic acid (EDTA), and benzoquinone (BQ) come from Sinopharm Chemical Reagent Co. Ltd., China. Urea and nitroblue tetrazolium (NBT) were purchased from Hushi Chemical Reagent Co. Ltd., Shanghai. Deionized water was used in all experiments.

2.2. Synthesis and Characterization of Photocatalysts. In a typical synthesis, 1.60 g titanium sulfate, 0.096 g thiourea, and 0.076 g urea were added to the mixture of 40 mL deionized water and 30 mL isopropanol. Then, the above obtained suspension was adjusted to pH 7 by addition of 1.0 M NaOH and subsequently put into a Teflon-lined stainless autoclave to hydrothermally treat at 140°C for 16 h. After completing this treatment, the autoclave was cooled to room temperature. Subsequently, 60 mL of 10.0 M NaOH was added into the above cooled autoclave and continued to hydrothermally treat in the same autoclave at 200°C for 48 h. The final obtained precipitate was then washed with deionized water, centrifuged, and transferred to 500 mL of 0.1 M HCl aqueous solution and kept constant stirring for 12 h. After HCl treatment, the obtained precipitate was further centrifuged and thoroughly washed with deionized water. The final obtained product (NS-TiO_2 NWs) was dried at 80°C for 24 h. The S-doped TiO_2 NWs were obtained by only adding thiourea as a sulfur source. All these two nanowires obtained by the above method were postheated in air atmosphere at 500–700°C for 2 h. The preparation method of NS-TiO_2 NPs is as follows. 1.6 g of titanium sulfate, 0.096 g thiourea, and 0.076 g urea were added to 40 mL deionized water and 30 mL 2-propanol. Then, the obtained suspension was adjusted to pH 12 by addition of 1.0 M NaOH and subsequently put into a Teflon-lined stainless autoclave to hydrothermally treat at 140°C for 16 h. The synthesized product was dried at 80°C for 24 h and calcined in air atmosphere at 600°C for 2 h.

Characterization such as crystal phase structure, morphology, element composition and optoelectronic properties of the samples were conducted by using X-ray diffraction (XRD, Bruker D8 Advance XRD diffractometer), environmental scanning electron microscopy (ESEM, Philips XL30 ESEM-FEG), transmission electron microscopy (TEM, JEM-2100HR, JEOL), X-ray photoelectron spectroscopy (XPS, Axis Ultra DLD, Kratos), and BET analyzer (ASAP2020M, Micromeritics), respectively.

2.3. Photocatalytic Activity Evaluation. A borosilicate glass dish (dia. 10 cm) was used as a photoreactor for photocatalytic evaluation. Twenty mL of initial concentration of 5 mg L^{-1} of atrazine solution was prepared using MilliQ grade water in the glass dish. Then, 0.02 g of doped TiO_2 NWs or doped TiO_2 NPs was placed in the solution to form the photocatalyst suspension. This suspension was magnetically stirred in the dark for 60 min before irradiation to ensure the establishment of an adsorption/desorption equilibrium of atrazine on the surface of photocatalyst.

Two 15 W fluorescent lamps (Philips, intensity: 3.99×10^{-4} W cm^{-2}) were used as a visible light source, and a UV block filter (UV420, Opticology) was mounted under the light source. A 0.5 mL sample was withdrawn at different time. The concentration of atrazine in the samples was quantified using high-performance liquid chromatography (HPLC, Agilent Series 1100) under the detectable wavelength of 220 nm for atrazine. An Agilent Eclipse C8 column (150 mm × 4.6 mm, particle size 5 μm) was employed. The flow phase is the mixture of 40% SQ water and 60% acetonitrile. The flow rate was 0.4 mL min^{-1} and the injection volume was 20 μL.

TOC was determined by Shimadzu TOC-VCPH analyzer. Photoluminescence (PL) technique with terephthalic acid (TA) as a probe molecule was used to detect the formation of free $^{\bullet}OH$ radicals on the surface of the visible-illuminated photocatalyst. Terephthalic acid readily reacts with $^{\bullet}OH$ and produces a highly fluorescent product, 2-hydroxyterephthalic acid, whose fluorescence emission spectra were recorded on a JASCO FP-6500 type fluorescence spectrophotometer excited at 315 nm.

3. Results and Discussion

3.1. Characterization of Synthesized Photocatalysts. The XRD results of NS-TiO_2 NWs (Figure 1) and S-TiO_2 NWs (see Figure S1 in Supplementary Material available online at http://dx.doi.org/10.1155/2014/425836. Figures S2 to S6 can also be seen in the Supplementary Material) indicate that both of the synthesized nanowires at the calcination of 500°C were a mixture of TiO_2 (B) and anatase phase. At the calcination of 700°C, two doped nanowires were composed of pure anatase phase and no rutile phase was found.

The as-synthesized NS-TiO_2 NWs (Figure 2) have a diameter of ~100–150 nm and a length of ~3–6 μm. It was also

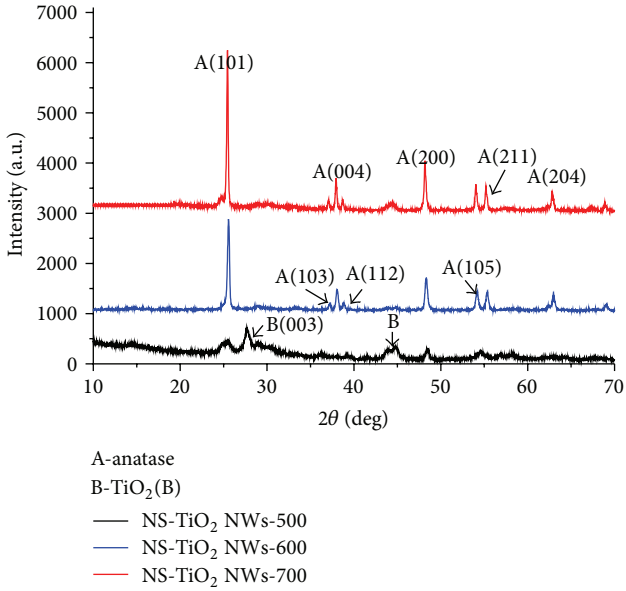

Figure 1: XRD of NS-TiO_2 NWs calcined at different temperature.

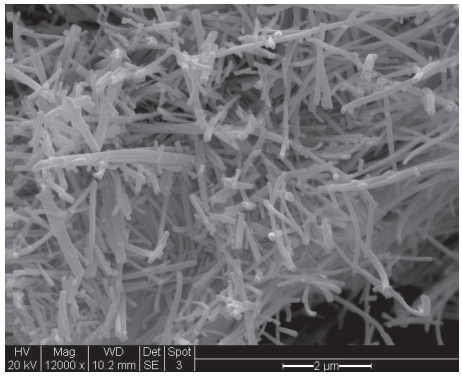

Figure 2: SEM image of NS-TiO_2 NWs.

confirmed that they have single-crystalline characteristics and grow along the [001] direction (Figure 3). The S-TiO_2 NWs have similar morphology structure (Figures S2 and S3). The content of sulfur in S-TiO_2 NWs and NS-TiO_2 NWs (Figure S4) is 0.43 at.% and 0.62 at.%, respectively. The N content is 2.38 at.% for NS-TiO_2 NWs. The average pore diameter and the BET surface area of S-TiO_2 NWs and NS-TiO_2 NWs (Figure S5) are about 35 nm and 22 nm and 39.8 $m^2\ g^{-1}$ and 35.1 $m^2\ g^{-1}$, respectively. The doped TiO_2 exhibited a noticeable shift of the optical absorption edges toward the visible region of the solar spectrum (Figure S6).

Recyclable experiments (Figure 4) exhibit that the aqueous suspension containing NS-TiO_2 NWs began to layer obviously by sedimentation at 5 min and was nearly clarified within 30 min, while P-25 (a commercial photocatalyst, Degussa) was still turbid. These observations indicate that the nanowire photocatalysts can be easily separated from the reaction system simply by sedimentation.

Cycling test was used to assess the reuse ability of photocatalysts. Photocatalytic degradation of atrazine over

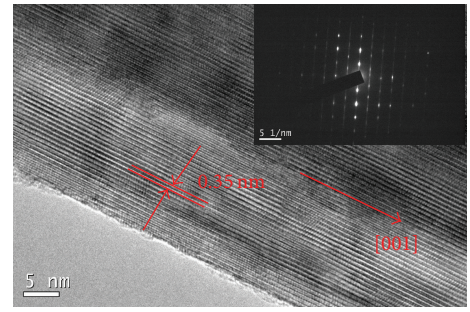

Figure 3: HRTEM and SAED (inset) of NS-TiO_2 NWs calcined at 600°C.

NS-TiO_2 NWs was performed for 5 cycles. The results shown in Figure 5 indicate that there is no obvious decrease in the photocatalytic activity over the test period which makes these nanowires attractive candidates as photocatalysts for industrial water purification.

3.2. Degradation of Atrazine. Adsorption tests (Figure 6) showed that adsorption-desorption equilibrium was reached within 60 min. All the tested photocatalysts showed similar adsorption capacity to atrazine molecules regardless of their composition, and the adsorption amount was less than 5%.

The photocatalytic activities of NS-TiO_2 NWs, S-TiO_2 NWs, and NS-TiO_2 NPs were investigated by degrading atrazine in aqueous solution under visible light. The NS-TiO_2 NPs were used as a reference to compare with the photocatalytic activities of doped TiO_2 NWs under the irradiation of visible light. All the doped photocatalysts showed enhanced photocatalytic activity for the degradation of atrazine under visible light irradiation (Figure 6). Among them, NS-TiO_2 NWs presented the highest performance, which can degrade more than 70% of atrazine within 6 h. In order to confirm the photocatalytic activity of doped TiO_2 NWs under visible light irradiation, a control experiment was also performed with the addition of TiO_2 NWs photocatalyst. There is no remarkable change of atrazine concentration in 6 h under the visible light condition. The fact indicates that the degradation of atrazine mainly resulted from the effective doping with sulfur or nitrogen/sulfur.

3.3. Kinetics and TOC Removal of Atrazine Degradation. The kinetics of photocatalytic degradation in each of the samples were investigated by applying the Langmuir-Hinshelwood first-order model as expressed by the following equation:

$$\ln\left(\frac{C_0}{C}\right) = kt, \tag{1}$$

where k is the first-order rate constant. For each sample, k was obtained by plotting $\ln(C_0/C)$ as a function of time, t (Figure 7 and Table 1).

From Table 1, it can be seen that the k value sequence is $k_{(\text{NS-TiO}_2\ \text{NWs})} > k_{(\text{S-TiO}_2\ \text{NWs})} > k_{(\text{NS-TiO}_2\ \text{NPs})}$ and the kinetic constant of NS-TiO_2 NWs is 1.5 times of that of NS-TiO_2 NPs. Obviously, NS-TiO_2 NWs showed the fastest degradation rate

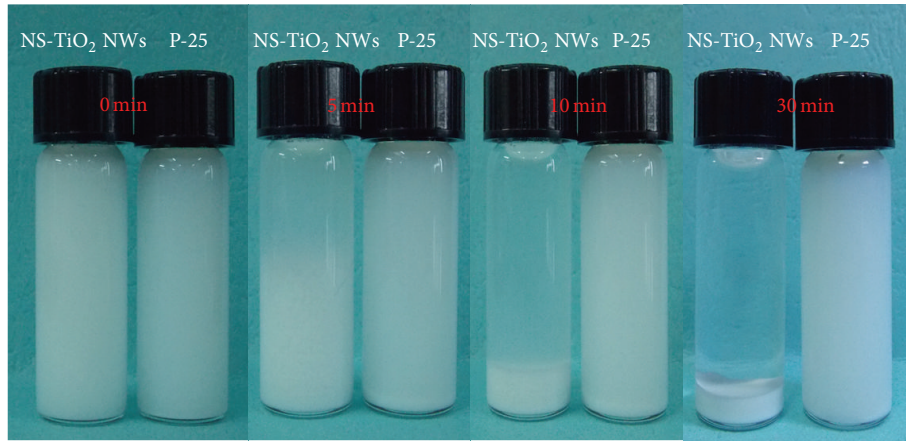

Figure 4: Sedimentation for 30 min in aqueous suspension of NS-TiO_2 NWs and P-25.

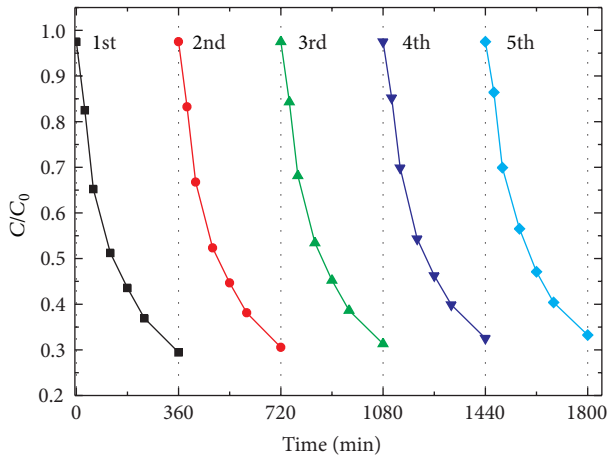

Figure 5: Photocatalytic activities of NS-TiO_2 NWs for atrazine degradation with 5 uses.

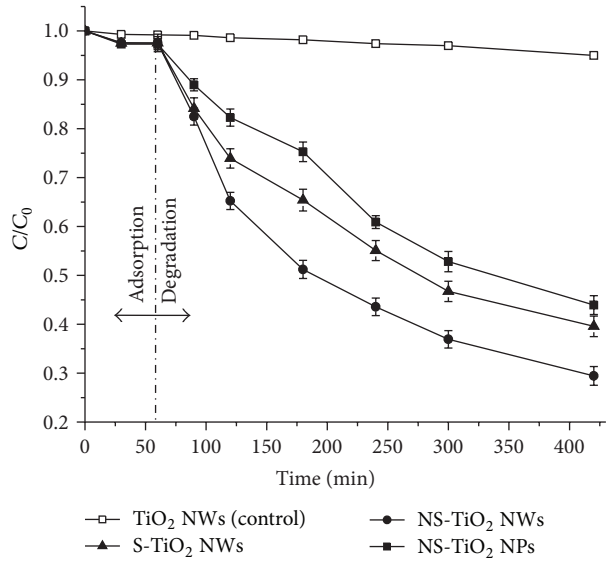

Figure 6: Photocatalytic degradation of atrazine irradiated by visible light.

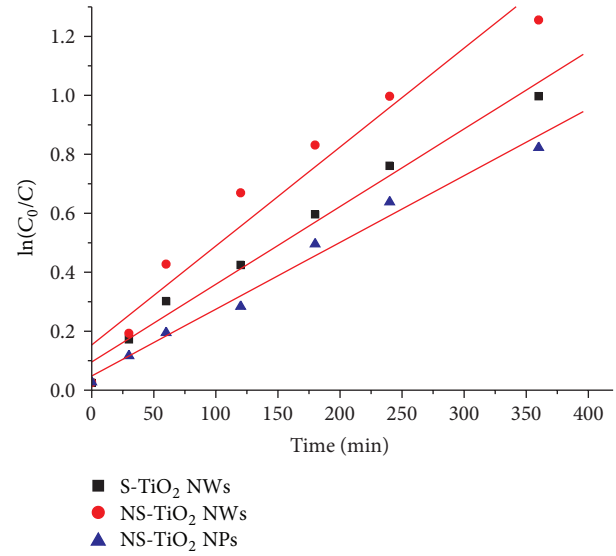

Figure 7: Kinetics of photocatalysts for the degradation of atrazine.

Table 1: Apparent first-order rate constants and TOC removal obtained from atrazine degradation by doped TiO_2 photocatalysts.

Sample	k (min^{-1})	Linear coefficient (R^2)	TOC removal (%)
NS-TiO_2 NPs	$(2.3 \pm 0.1) \times 10^{-3}$	0.9858	48
S-TiO_2 NWs	$(2.6 \pm 0.2) \times 10^{-3}$	0.9834	55
NS-TiO_2 NWs	$(3.4 \pm 0.3) \times 10^{-3}$	0.9617	63

among all the tested photocatalysts for atrazine degradation under visible light irradiation.

Figure 8 and Table 1 show the TOC removal profile by using these samples for mineralization of 5 mg L^{-1} atrazine with time. It is observed that NS-TiO_2 NWs mineralized atrazine much faster than the other two samples at the given time and achieved 63% of atrazine mineralization within 6 h. The results are in accordance with atrazine degradation. The value differences between atrazine degradation and

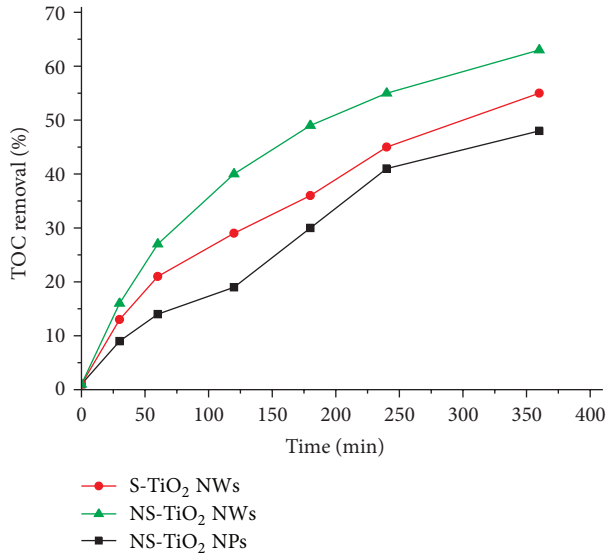

FIGURE 8: TOC removal rate as a function of irradiation time during mineralization of 5 mg L^{-1} atrazine.

mineralization mean that atrazine is not easy to be completely transformed to carbon dioxide and water [3].

It is worth noticing that photocatalytic activity of doped TiO_2 NWs is higher than that of doped TiO_2 NPs. It can be attributed to the higher charge carrier mobility and lower carrier recombination rate of nanowires than to those of nanoparticles, which is helpful for the separation of electron/hole pairs and electron transfer causing more radical species with strong oxidation capability. The speed of electron diffusion across nanoparticle junctions is several orders of magnitude smaller than that of nanowire due to frequent electron trapping at the junctions of nanoparticles and separated charges are easily recombined before they reach the surface of nanoparticles [21].

3.4. Reactive Oxygen Species (ROS). Atrazine was rarely adsorbed on TiO_2 (Figure 6) and the structure of atrazine did not facilitate itself to undergo nonradical interface reaction. In order to further confirm that, the role of the active species, such as electrons/holes, $^{\bullet}OH$, and $O_2^{\bullet-}$, was investigated in the photocatalytic degradation process. Figure 9 exhibited the photocatalytic activity of NS-TiO_2 NWs and NS-TiO_2 NPs toward the atrazine degradation after different radical scavengers were added. TBA is considered as an excellent capturer of $^{\bullet}OH$ and can be easily oxidized by $^{\bullet}OH$ [22]. The addition of TBA (5×10^{-3} mol L^{-1}) led to the most inhibition of the atrazine degradation, illuminating that $^{\bullet}OH$ played the most important role in the photocatalytic degradation process. Holes are another reactive species in photocatalytic reactions, which can be captured by EDTA [23]. After EDTA was added into the system (1×10^{-3} mol L^{-1}), the photocatalytic degradation process was remarkably inhibited. It is obviously observed that the degradation using NS-TiO_2 NPs was influenced greater than that using NS-TiO_2 NWs when the individual same amount of TBA or EDTA was added into the aqueous solution. The result indicated that NS-TiO_2 NWs possibly generated more $^{\bullet}OH$ and holes at the same given time.

Moreover, dissolved O_2 is an electron-capturer to produce a variety of active oxygen species and promotes the degradation process. In order to evaluate the role of dissolved O_2 in the reaction, N_2 was bubbled through the suspension at the rate of 5 mL min^{-1} to ensure that the reaction was operated without O_2. BQ had the ability to trap $O_2^{\bullet-}$ by a simple electron transfer mechanism [24]. The addition of BQ (0.2 mg) did not significantly inhibit atrazine degradation, indicating that $O_2^{\bullet-}$ in the aqueous was not the main reactive species during the degradation.

Based on the above analysis, it could be concluded that the degradation of atrazine was driven mainly by $^{\bullet}OH$ and holes, but the role of $O_2^{\bullet-}$ played in the degradation was not completely ignored.

As mentioned above, $^{\bullet}OH$ radicals played the most important role in the photocatalytic degradation process. PL-TA technique was used to monitor the amount of $^{\bullet}OH$ in the photocatalytic systems, which has been widely used in the detection of $^{\bullet}OH$ [25]. Figure 10(a) showed the PL intensity of NS-TiO_2 NWs, S-TiO_2 NWs, and NS-TiO_2 NPs in aqueous TA solution. It was found that the intensity of NS-TiO_2 NWs was higher than those of S-TiO_2 NWs and NS-TiO_2 NPs, indicating that NS-TiO_2 NWs produced more amount of $^{\bullet}OH$ at the same given time.

To further ascertain the change of $O_2^{\bullet-}$, a colorless molecular probe, NBT, was chosen to quantify the $O_2^{\bullet-}$ concentration produced by NS-TiO_2 NWs, S-TiO_2 NWs, and NS-TiO_2 NPs under visible light irradiation. Figure 11 showed the variation of NBT concentration, and the decrease of NBT concentration indicated the generation of $O_2^{\bullet-}$. It was found that the production rate of $O_2^{\bullet-}$ for NS-TiO_2 NWs was much higher than those of S-TiO_2 NWs and NS-TiO_2 NPs (Figure 10(b)).

3.5. Degradation Mechanism. The excellent photocatalytic activity of NS-TiO_2 NWs is primarily attributed to three reasons. Firstly, according to the results of XPS (Figure S4), the sulfur atoms present a peak at about 164 eV corresponding to the formation of Ti-S bond. The substitution of sulfur at the O sites could significantly modify the electronic structure of TiO_2 due to a larger ionic radius of S than that of O. When TiO_2 is doped with sulfur, the S 2p states are somewhat delocalized, thus greatly contributing to the formation of VB with O 2p and Ti 3d states. Consequently, the mixing of the S 2p states with VB results in the increase of the width of the VB, which decreases the band gap energy and finally contributes to the band gap narrowing (Scheme 1). This in turns results in the improvement of photocatalytic activity of the catalysts [26, 27].

This newly developed S-TiO_2 NWs, which incorporated S atoms into the lattice of TiO_2, results in increase in photoinduced electrons, leading to a remarkable increase in electron-hole separation and a concomitant decrease in charge carrier recombination. The S-TiO_2 NWs also caused the creation of oxygen defects in anatase lattice, which is important to show visible-light response. Thus, the sulfur

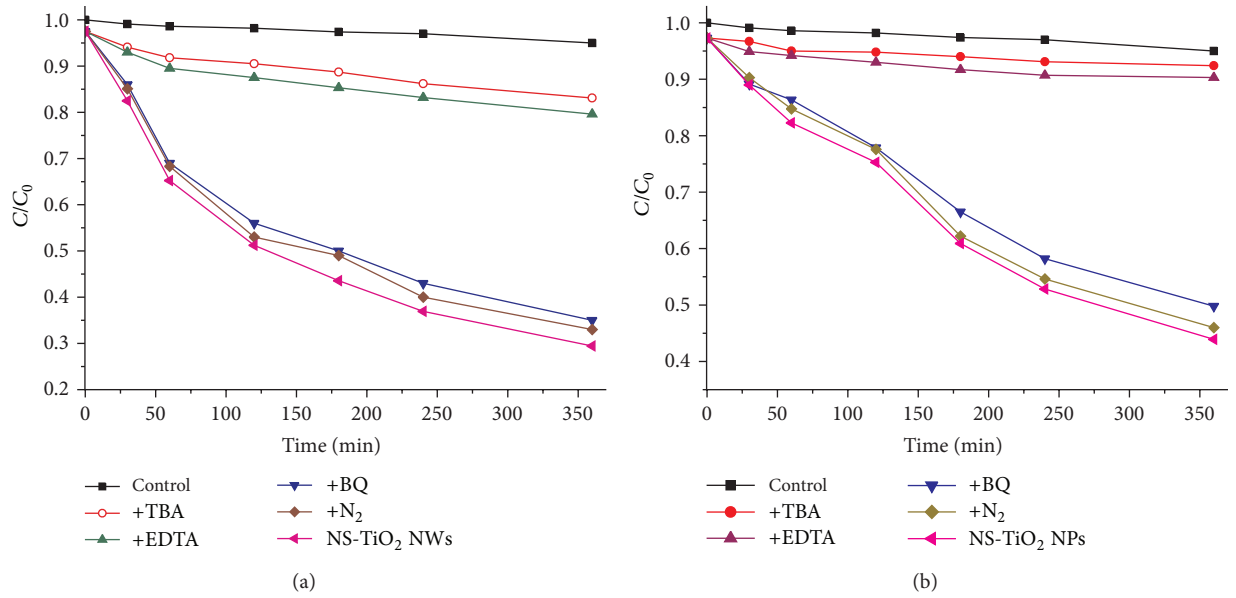

Figure 9: Atrazine degradation of (a) NS-TiO_2 NWs and (b) NS-TiO_2 NPs under different conditions under visible light irradiation.

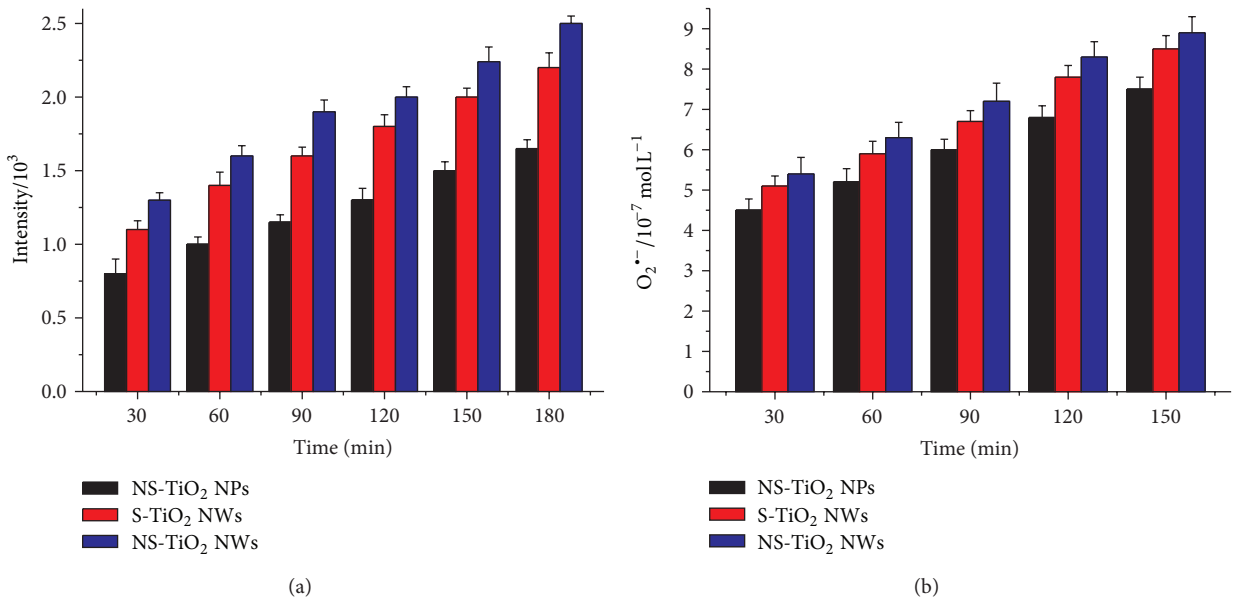

Figure 10: (a) $^{\bullet}OH$-trapping PL intensity of NS-TiO_2 NPs, S-TiO_2 NWs, and NS-TiO_2 NWs in TA solution and (b) change of $O_2^{\bullet-}$ concentration for NS-TiO_2 NPs, S-TiO_2 NWs, and NS-TiO_2 NWs.

dopants can work partially with oxygen to enhance the activity of the photocatalyst [28]. In this case, the contribution of S doping for these three photocatalysts for the enhancement of photocatalytic activity is approximately the same.

For NS-TiO_2 NWs and NS-TiO_2 NPs, the role of N doping is similar to S doping in narrowing the band gap and separating electron-hole pairs. Thus, we ascribe the enhancement of photocatalytic activity to the synergistic effect of N and S doping. We infer that the energy level position of electron or hole produced by visible light absorption in NS-TiO_2 NWs and NS-TiO_2 NPs is more conducive to the generation of reactive groups than that of S-TiO_2 NWs. Therefore, the degradation rates of NS-TiO_2 NWs and NS-TiO_2 NPs were faster than that of S-TiO_2 NWs for atrazine degradation from the analysis of N and S doping.

Undoubtedly, according to the overall degradation results (Figure 6), the photocatalysts with nanowire structure possess the advantage over that with nanoparticle structure as though the degradation rate of NS-TiO_2 NPs was faster than that of S-TiO_2 NWs due to the N and S doping. This can be attributed to higher charge carrier mobility and lower carrier recombination rate of nanowire-structure material,

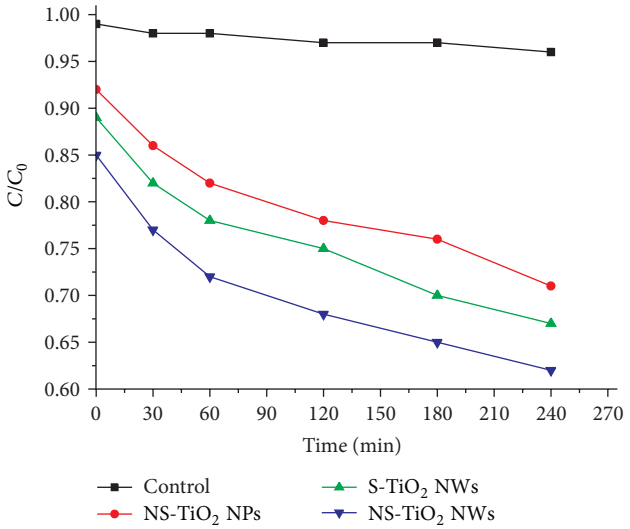

Figure 11: The variation in the concentration of NBT with NS-TiO_2 NPs, S-TiO_2 NWs, and NS-TiO_2 NWs samples under visible light irradiation.

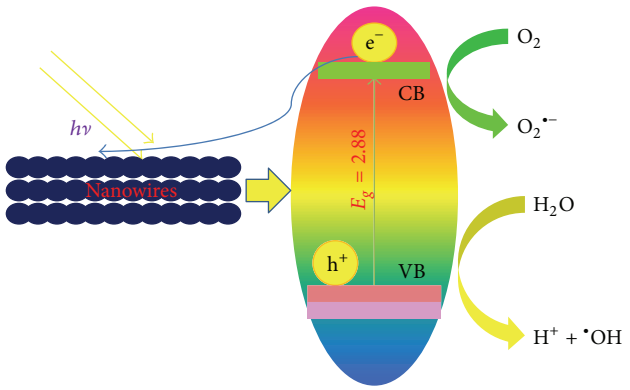

Scheme 1: Electronic structure of NS-TiO_2 NWs.

which has the advantage of providing a pathway of transporting charges without grain boundaries and junctions. Once electrons are injected to the conduction band of titanium dioxide, recombination can be minimized due to its relatively wide band gap.

Secondly, in this study, pure anatase phase is still present at 600°C (even 700°C) as shown in Figure 1, which usually occurs in the transformation of anatase to rutile in pure titanium or doped titanium nanoparticles at around 600°C [29]. TiO_2 with rutile phase has been confirmed to have weaker photocatalytic ability for contaminant degradation compared to TiO_2 with anatase phase. In this case, the retention of the anatase phase up to 700°C can be attributed to the presence of TiO_2 (B) phase. From these observations, it can be concluded that extending the anatase-to-rutile transformation temperature above 600°C enables us to achieve enhanced photocatalytic activity.

Finally, from the HRTEM analyses, the growth of doped TiO_2 NWs is along the [001] crystallographic direction. According to the model of anatase TiO_2 [30], this means that the {001} planes of anatase were preferentially exposed to side surfaces of the nanowire. Liu et al. [31] have demonstrated that TiO_2 materials with preferred {001} facets have an enhanced photocatalytic efficiency for degradation of Methylene Blue dye. Consequently, the high photocatalytic activity of TiO_2 NWs could also be partially attributed to these reactive facets. However, further work is required to elucidate the exact role of {001} planes in enhancing the nanowires' activity.

4. Conclusion

In this study, the NS-TiO_2 NWs calcined at 600°C exhibited the best photocatalytic activity for the degradation of atrazine under visible light irradiation compared to NS-TiO_2 NPs and S-TiO_2 NWs. TOC removal also presented the similar result and achieved 63% of atrazine mineralization within 6 h. Reactive species quantities such $^{\bullet}OH$ and $O_2^{\bullet-}$ generated by NS-codoped TiO_2 NWs were much more than those of S-TiO_2 NWs and NS-TiO_2 NPs during the photocatalytic process. These results were mainly attributed to the synergistic effect of N and S doping in narrowing the band gap, remarkable increase in electron-hole separation, extending the anatase-to-rutile transformation temperature above 600°C, and preferentially exposing high reactive {001} crystal facets of anatase.

Conflict of Interests

The authors declare that there is no conflict of interests regarding the publication of this paper.

Acknowledgment

This work was supported by the Natural Science Foundation of China (41372050).

References

[1] USEPA, *Atrazine Chemical Summary, Toxicity and Exposure Assessmentfor Children's Health*, 2007, http://www.epa.gov/teach/chem_summ/Atrazine_summary.pdf.

[2] M. Graymore, F. Stagnitti, and G. Allinson, "Impacts of atrazine in aquatic ecosystems," *Environment International*, vol. 26, no. 7-8, pp. 483–495, 2001.

[3] N. Borràs, R. Oliver, C. Arias, and E. Brillas, "Degradation of atrazine by electrochemical advanced oxidation processes using a boron-doped diamond anode," *Journal of Physical Chemistry A*, vol. 114, no. 24, pp. 6613–6621, 2010.

[4] M. H. Pérez, G. Peñuela, M. I. Maldonado et al., "Degradation of pesticides in water using solar advanced oxidation processes," *Applied Catalysis B: Environmental*, vol. 64, no. 3-4, pp. 272–281, 2006.

[5] C. L. Bianchi, C. Pirola, V. Ragaini, and E. Selli, "Mechanism and efficiency of atrazine degradation under combined oxidation processes," *Applied Catalysis B: Environmental*, vol. 64, no. 1-2, pp. 131–138, 2006.

[6] J. De Laat, H. Gallard, S. Ancelin, and B. Legube, "Comparative study of the oxidation of atrazine and acetone by H_2O_2/UV,

Fe(III)/UV, Fe(iii)/H_2O_2/UV and Fe(II) or Fe(III)/H_2O_2," *Chemosphere*, vol. 39, no. 15, pp. 2693–2706, 1999.

[7] S. M. Arnold, W. J. Hickey, and R. F. Harris, "Degradation of atrazine by Fenton's reagent: condition optimization and product quantification," *Environmental Science and Technology*, vol. 29, no. 8, pp. 2083–2089, 1995.

[8] K. H. Chan and W. Chu, "Atrazine removal by catalytic oxidation processes with or without UV irradiation: part II: an analysis of the reaction mechanisms using LC/ESI-tandem mass spectrometry," *Applied Catalysis B: Environmental*, vol. 58, no. 3-4, pp. 165–174, 2005.

[9] A. Ventura, G. Jacquet, V. Camel, and A. Bermond, "Comparison between the classical and the electrochemical Fenton systems for atrazine degradation in acidic medium," *Journal of Advanced Oxidation Technologies*, vol. 5, no. 1, pp. 113–120, 2002.

[10] S. Nélieu, L. Kerhoas, and J. Einhorn, "Degradation of atrazine into ammeline by combined ozone/hydrogen peroxide treatment in water," *Environmental Science & Technology*, vol. 34, no. 3, pp. 430–437, 2000.

[11] J. Andersen, M. Pelaez, L. Guay, Z. Zhang, K. O'Shea, and D. D. Dionysiou, "NF-TiO_2 photocatalysis of amitrole and atrazine with addition of oxidants under simulated solar light: emerging synergies, degradation intermediates, and reusable attributes," *Journal of Hazardous Materials*, vol. 260, pp. 569–575, 2013.

[12] B. Yu, W. M. Lau, and J. Yang, "Preparation and characterization of N-TiO_2 photocatalyst with high crystallinity and enhanced photocatalytic inactivation of bacteria," *Nanotechnology*, vol. 24, no. 33, Article ID 335705, 2013.

[13] Y. A. Shaban, M. A. El Sayed, A. A. El Maradny, R. K. Al Farawati, and M. I. Al Zobidi, "Photocatalytic degradation of phenol in natural seawater using visible light active carbon modified (CM)-n-TiO_2 nanoparticles under UV light and natural sunlight illuminations," *Chemosphere*, vol. 91, no. 3, pp. 307–313, 2013.

[14] X. Wu, S. Yin, Q. Dong et al., "Synthesis of high visible light active carbon doped TiO_2 photocatalyst by a facile calcination assisted solvothermal method," *Applied Catalysis B: Environmental*, vol. 142-143, pp. 450–457, 2013.

[15] Y. Xia, Y. Jiang, F. Li, M. Xia, B. Xue, and Y. Li, "Effect of calcined atmosphere on the photocatalytic activity of P-doped TiO_2," *Applied Surface Science*, vol. 289, pp. 306–315, 2014.

[16] W. Buda and B. Czech, "Preparation and characterization of C,N-codoped TiO_2 photocatalyst for the degradation of diclofenac from wastewater," *Water Science and Technology*, vol. 68, no. 6, pp. 1322–1328, 2013.

[17] H. Bai, K. S. Y. Kwan, Z. Liu, X. Song, S. S. Lee, and D. D. Sun, "Facile synthesis of hierarchically meso/nanoporous s- and c-codoped TiO_2 and its high photocatalytic efficiency in H_2 generation," *Applied Catalysis B: Environmental*, vol. 129, pp. 294–300, 2013.

[18] M. Pelaez, A. A. de la Cruz, E. Stathatos, P. Falaras, and D. D. Dionysiou, "Visible light-activated N-F-codoped TiO_2 nanoparticles for the photocatalytic degradation of microcystin-LR in water," *Catalysis Today*, vol. 144, no. 1-2, pp. 19–25, 2009.

[19] W. Wang, Y. Ni, C. Lu, and Z. Xu, "Hydrogenation temperature related inner structures and visible-light-driven photocatalysis of N-F co-doped TiO_2 nanosheets," *Applied Surface Science*, vol. 290, pp. 125–130, 2014.

[20] A. C. Fisher, L. M. Peter, E. A. Ponomarev, A. B. Walker, and K. G. U. Wijayantha, "Intensity dependence of the back reaction and transport of electrons in dye-sensitized nanocrystalline TiO_2 solar cells," *Journal of Physical Chemistry B*, vol. 104, no. 5, pp. 949–958, 2000.

[21] H. Yin, G. Ding, B. Gao, F. Huang, X. Xie, and M. Jiang, "Synthesis of ultrafine titanium dioxide nanowires using hydrothermal method," *Materials Research Bulletin*, vol. 47, no. 11, pp. 3124–3128, 2012.

[22] Y. Zhang, J. W. C. Wong, P. Liu, and M. Yuan, "Heterogeneous photocatalytic degradation of phenanthrene in surfactant solution containing TiO_2 particles," *Journal of Hazardous Materials*, vol. 191, no. 1–3, pp. 136–143, 2011.

[23] Y. Hou, X. Li, Q. Zhao, G. Chen, and C. L. Raston, "Role of hydroxyl radicals and mechanism of escherichia coli inactivation on Ag/AgBr/TiO_2 nanotube array electrode under visible light irradiation," *Environmental Science and Technology*, vol. 46, no. 7, pp. 4042–4050, 2012.

[24] J. Yang, C. Chen, H. Ji, W. Ma, and J. Zhao, "Mechanism of TiO_2-assisted photocatalytic degradation of dyes under visible irradiation: photoelectrocatalytic study by TiO_2-film electrodes," *Journal of Physical Chemistry B*, vol. 109, no. 46, pp. 21900–21907, 2005.

[25] J. C. Barreto, G. S. Smith, N. H. P. Strobel, P. A. McQuillin, and T. A. Miller, "Terephthalic acid: a dosimeter for the detection of hydroxyl radicals in vitro," *Life Sciences*, vol. 56, no. 4, pp. PL89–PL96, 1994.

[26] S. T. Hussain, K. Khan, and R. Hussain, "Size control synthesis of sulfur doped titanium dioxide (anatase) nanoparticles, its optical property and its photo catalytic reactivity for CO_2 + H_2O conversion and phenol degradation," *Journal of Natural Gas Chemistry*, vol. 18, no. 4, pp. 383–391, 2009.

[27] K. Li, T. Chen, L. Yan et al., "Design of graphene and silica co-doped titania composites with ordered mesostructure and their simulated sunlight photocatalytic performance towards atrazine degradation," *Colloid Surface A*, vol. 422, pp. 90–99, 2013.

[28] J. Wang, H. Li, H. Li, S. Yin, and T. Sato, "Preparation and characterization of titania/tetratitanate nanocomposites," *Solid State Sciences*, vol. 11, no. 5, pp. 988–993, 2009.

[29] W. Li, Y. Bai, C. Liu et al., "Highly thermal stable and highly crystalline anatase TiO_2 for photocatalysis," *Environmental Science and Technology*, vol. 43, no. 14, pp. 5423–5428, 2009.

[30] C. K. Nguyen, H. G. Cha, and Y. S. Kang, "Axis-oriented, anatase TiO_2 single crystals with dominant 001 and 100 facets," *Crystal Growth & Design*, vol. 11, no. 9, pp. 3947–3953, 2011.

[31] M. Liu, L. Piao, L. Zhao et al., "Anatase TiO_2 single crystals with exposed 001 and 110 facets: facile synthesis and enhanced photocatalysis," *Chemical Communications*, vol. 46, no. 10, pp. 1664–1666, 2010.